



Soft Matter

**Preferential electrostatic interactions of phosphatidic acid
with arginines**

Journal:	<i>Soft Matter</i>
Manuscript ID	SM-ART-01-2024-000088
Article Type:	Paper
Date Submitted by the Author:	20-Jan-2024
Complete List of Authors:	Thomas, Nidhin; University of Houston Combs, Wesley; University of Houston Mandapapu, Kranthi; UC Berkeley, Chemistry Agrawal, Ashutosh; University of Houston System,

SCHOLARONE™
Manuscripts

Cite this: DOI: 00.0000/xxxxxxxxxx

Preferential electrostatic interactions of phosphatidic acid with arginines[†]

Nidhin Thomas,^a Wesley Combs,^a Kranthi K. Mandadapu,^{bc} and Ashutosh Agrawal^{*a}

Received Date

Accepted Date

DOI: 00.0000/xxxxxxxxxx

Phosphatidic acid (PA) is an anionic lipid that preferentially interacts with proteins in a diverse set of cellular processes such as transport, apoptosis, and neurotransmission. One such interaction is that of the PA lipids with the proteins of voltage-sensitive ion channels. In comparison to several other similarly charged anionic lipids, PA lipids exhibit much stronger interactions. Intrigued and motivated by this finding, we sought out to gain deeper understanding into the electrostatic interactions of anionic lipids with charged proteins. Using voltage sensor domain (VSD) of the KvAP channel as a model system, we performed long-timescale atomistic simulations to analyze interactions of POPA, POPG, and POPI lipids with arginines (ARG). Our simulations reveal two mechanisms. First, POPA is able to interact not only with surface ARGs but is able to snorkel and interact with a buried arginine. POPG and POPI lipids on the other hand show weak interactions even with both the surface and buried ARGs. Second, deprotonated POPA with -2 charge is able to break the salt-bridge connection between VSD protein segments and establish its own electrostatic bond with the ARG. Based on these findings, we propose a headgroup size hypothesis for preferential solvation of proteins by charged lipids. These findings may be valuable in understanding how PA lipids could be modulating kinematics of transmembrane proteins in cellular membranes.

1 Introduction

Phosphatidic acid (PA) is a negatively charged lipid which is a key intermediate in the synthesis of membrane glycerophospholipids^{1,2}. PA lipids acts as signaling molecules influencing membrane properties, membrane structure, recruitment and insertion of proteins, and activation of enzymes. These PA-dependent processes play a crucial role in endocytosis, exocytosis, apoptosis, and neurotransmission³.

One specific class of preferential interactions that PA lipids exhibit is with the voltage-sensitive ion channels^{4–10}. POPA lipids have been shown to inhibit the gating of KvAP and Kv Chimera channels⁴. POPA lipids have also been found to stabilize the tetrameric assembly of KcsA channels^{5,11,12}. Going beyond Kv channels, POPA lipids have been shown to inhibit the gating of epithelial Na channels¹³. There are two key features that make the interactions of PA with Kv channels stand out. First, POPA is able to influence the gating of Kv channels at a mere concentration of 5%⁴. Second, PA has a more pronounced effect on Kv

channel gating than other similarly charged lipids such as POPG, POPI and POPS and anionic lipids such as cardiolipin and PIP with higher negative charges⁴. PA lipids also show stronger interaction with KcsA channels than POPG lipids^{5,14,15}.

The above experimental findings lead to a natural question: why do POPA lipids selectively interact with charged proteins like voltage-sensitive ion channels? Mutagenesis experiments on archeal KvAP channel⁴ show that POPA phosphate group interacts with non-annular arginines. Interactions of POPA lipids with arginines has also been shown for KcsA channel¹⁶. These interactions are likely governed by the strong affinity between phosphate and guanadinium that is well established¹⁷. In addition, PA lipids exhibit an electrostatic-hydrogen bond switch that leads to deprotonation and an increase in the headgroup charge^{2,18–21}. Since the pK_{a2} of PA is close to the physiological pH of cells (6.6–7.9)^{2,19,22–25}, there is a high likelihood of finding a PA lipids with -2 charge. In addition, presence of multiple positively charged residues further lowers the pK_{a2} of PA lipids^{21,26,27}. As VSD possesses several arginines, it is plausible that PA lipids exhibit an increased charge of -2 in the channel environment.

While the studies above provide the basis for PA lipids to interact favorably with charged proteins, the consequences of the molecular interactions are not well quantified. For example, the extent to which phosphate-guanadinium affinity allows anionic lipids to interact with positive residues in charged proteins is not known. How is this interaction dependent on the depth of the

^a Department of Mechanical Engineering, University of Houston, Houston, TX, 77204, USA. E-mail: ashutosh@uh.edu

^b Department of Chemical & Biomolecular Engineering, University of California, Berkeley, CA 94720, USA

^c Chemical Sciences Division, Lawrence Berkeley National Laboratory, CA 94720, USA

[†] Electronic Supplementary Information (ESI) available: See DOI: 10.1039/cXsm00000x/

positive residue in the membrane? How do these interactions manifest in the case of other anionic lipids such as POPG and POPI? Do these interactions explain the reduced interactions of these lipids with VSDs despite having similar phosphate groups? What are the consequences of increased headgroup charge on the interaction of PA lipids with the positive residues? Does it enable new electrostatic interactions or stabilize existing interactions?

To probe into the questions outlined above, we performed long time scale all-atom molecular dynamics simulations to investigate the interactions of POPA, POPG, and POPI with the VSD of KvAP channel, as a model protein system. Ion channels serve as a good model system as they have a cluster of arginines located on a single alpha helix. This enables investigation of PA-ARG interactions as a function of ARG depth in the membrane. Because of multiple charges, we also expect the probability of deprotonation of PA lipid to be higher in the physiological setting². We, therefore, also examined the interactions of PA lipids with pre-assigned two negative charges with the VSD. Our studies reveal that POPA with a unit charge is able to access both the surface ARGs (R117, R120) and the buried ARG (R123) by snorkeling into the bilayer. Despite similar charges, POPG and POPI lipids are unable to snorkel and interact with R123, and show a much weaker interaction even with the surface ARGs. POPA with two unit charges, on the other hand, is able to break a salt-bridge connection between two alpha helices in the VSD and establish its own electrostatic bond with the buried ARG R123. These findings give insights into potential mechanisms by which POPA is selectively able to interact with charged proteins. These findings might be valuable in understanding preferential interactions of POPA with voltage-sensitive ion channels and other charged proteins present in cellular membranes.

2 Methods and Materials

2.1 Equilibrium MD Simulations

We used CHARMM-GUI^{28,29} to create an all-atom model of initial configurations. The cryo-EM structure of the voltage sensor domain (VSD) of the KvAP channel in open configuration (PDB ID: 6UWM) was obtained from³⁰. Seven systems were simulated to study the effect of anionic lipids in KvAP channel (see Table S1, ESI[†]). In the first system, VSD was inserted into pure POPC lipid bilayer. 200 POPC lipids were used to create the bilayer. 100 POPC lipids were used to create each top and bottom leaflets. The additional lipids were used to balance the area per lipid of each leaflet in order to maintain zero surface tension in each leaflet. VSD was inserted into the bilayer using CHARMM-GUI and used PPM server to determine the placement of the protein. Other systems were created in CHARMM-GUI by replacing 25% of POPC with anionic lipids (POPA, POPG and POPI). We performed all the simulations at 303K temperature to ensure that the lipid bilayers are above the phase transition temperature in the liquid disordered state. This is important to capture the dynamics of lipid-protein interactions. In addition, simulations performed at 303K are not expected to lead to protein denaturation as it falls well within the physiological range. 0.150 mM KCl was added to the system to neutralize the sys-

tem. We used CHARMM36m, CHARMM36 force fields^{31,32} for protein and lipids, respectively. TIP3P water model³³ was used throughout the simulation along with CHARMM36 force field for ions. Simulations were run in GROMACS 2018.3³⁴. The force field parameters used for POPA⁽⁻²⁾ was derived from POPA and DOPP⁽⁻²⁾ lipids. The partial charge distribution of POPA⁽⁻²⁾ lipid headgroup is provided in the ESI[†]. Considering the charge of POPA⁽⁻²⁾ and DOPP⁽⁻²⁾ lipids, only 10% POPA⁽⁻²⁾ or DOPP⁽⁻²⁾ lipids were added to the system. Additional MD simulations were performed with different initial velocity distribution to reproduce the results. Each system was simulated for 1.5 microseconds after reaching equilibration. Initial 200 ns of the production runs were discarded to account for the equilibration.

2.2 Umbrella Sampling Simulations

Equilibrated structures from the MD simulations were used as the initial structures for the pulling simulations. We performed pulling simulations of lipids to obtain the initial structures required for each umbrella sampling simulation window. The pulling simulation procedure and the parameters are described in detail in the ESI[†]. After the initial pulling simulations, structures with 0.1 nm increment in the reaction coordinates were chosen for the umbrella sampling. Each window was simulated for 200 ns and the final 50 ns were chosen for the free energy analysis. We used 'gmx wham' tool to calculate the free energy profiles and the error bars. The parameters used for the umbrella sampling and free energy calculations are provided in the ESI[†]. The results were analyzed using in-house scripts.

3 Results

3.1 POPA lipids can snorkel in lipid bilayers to establish electrostatic interactions with buried ARG

We began by studying the interactions between the KvAP VSD and POPA lipids using all-atom molecular simulations. We simulated the cryo-EM structure of the VSD of KvAP channel³⁰, in a mixed bilayer comprising of 75% POPC lipids and 25% POPA lipids. Fig. 1 shows a simulated system with the VSD embedded in the mixed bilayer (POPC lipids are shown in dark gray and POPA lipids are shown in gold). The S4 segment of the VSD carries the positively charged arginines. The details of the MD simulations are provided in the Methods section and the ESI[†].

We computed the two-dimensional areal density plots of POPA and POPC lipids around the VSD in order to quantify the local distribution of lipids around the VSD. The areal density is defined by 2D number density of the oxygen atoms of the phosphate groups in the outer leaflet of the bilayer. Fig. 2a and 2b show the density plots of POPA and POPC lipids in the outer leaflet, respectively. The POPA plot shows three hotspots in the close vicinity of S4 segment. In comparison, POPC lipids do not possess any hotspots in the vicinity of S4. The yellow regions in the POPC plot are located away from the S4 segment. This demonstrates that the POPA lipids have a propensity to preferentially aggregate near the S4 segment, unlike POPC, and enter the solvation shell of the VSD. The 2D number density plots of POPC and POPA lipids in the reproduction run are shown in Fig. S1 (ESI[†]).

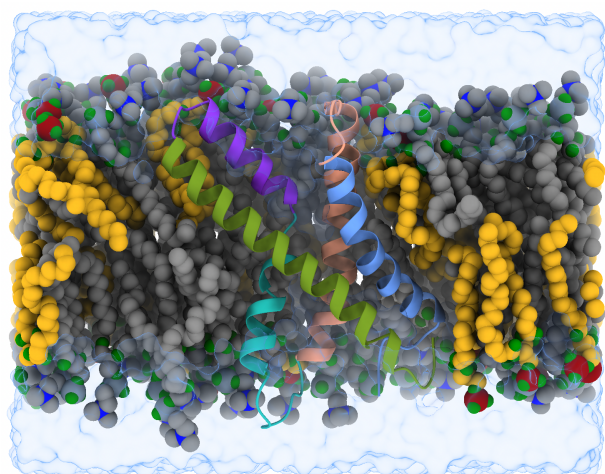


Fig. 1 Molecular dynamics set-up used to study lipid-Kv channel interactions. Voltage sensor domain (VSD) of the KvAP channel is placed inside a POPC(75%)-POPA(25%) membrane. POPC and POPA lipids are colored gray and gold, respectively. Nitrogen atoms of POPC lipids are colored blue, phosphorus atoms of POPA are shown in red, and oxygen atoms of POPC and POPA are colored green. The VSD protein segment S1 is shown in light blue, S2 is colored salmon, S3a is in cyan, S3b is in purple and S4 is shown in green.

To comprehend POPA-VSD interactions, we analyzed the POPA-ARG interactions. Fig. 3a shows POPA lipids (in yellow) in close proximity of ARGs R117, R120, and R123. The first two ARGs are at the level of lipid-water interface and their interaction with POPA gives rise to the left two hotspots in Fig. 2a. Remarkably, the third ARG R123 is buried into the bilayer and POPA is able to snorkel and interact with it. This interaction gives rise to the rightmost hotspot in Fig. 2a. The plot shows direct electrostatic interactions between the phosphate (P) groups of the POPA lipids and the ARG residues. Specifically, we find that the negatively charged phosphoryl oxygen atoms (O11, O12, O13, O14) in the phosphate group of the POPA lipids interact with the positively charged nitrogen atoms (N_{ϵ} , $N_{\eta 1}$, $N_{\eta 2}$) in the guanidinium group of the S4 helix. The atomistic representation of the lipid headgroup and the arginine side chains are shown in Fig. S2 (ESI[†]).

In order to ensure that these interactions are strong, we computed the distances between the headgroup oxygen atom of clustered POPA lipids and the nitrogen atom of guanidinium side chains of ARG residues as a function of time from two independent simulations (Fig. 3b and Fig. 3c). As the molecular interactions are stochastic in nature, analyzing data from more than one simulation presents a more accurate picture. Several key observations can be made from the time plots. First, POPA lipids are able to establish electrostatic interaction with all three ARGs. This is evident from the fact that the distance plots associated with all the three ARGs show flattened phases. Second, POPA is able to maintain stable interactions with at least two POPA lipids during the entire simulated time frame. In Fig. 3b, prior to 1000 ns interactions with all three ARGs are stable, and after 1000 ns interactions with R117 and R120 continue to remain stable. In Fig. 3c, interactions with R123 and R120 remain stable throughout the simulation time. Third, remarkably, POPA is able to maintain

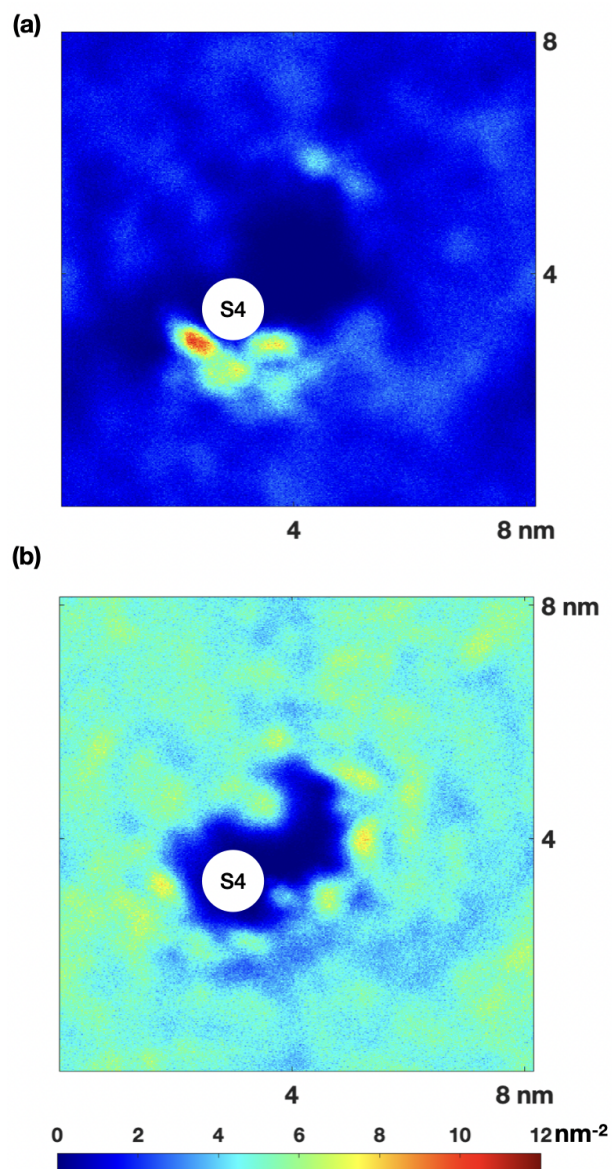


Fig. 2 2D density plots of (a) POPA lipids and (b) POPC lipids in the outer membrane leaflet of POPC(75):POPA(25) system. POPA lipids show three hotspots (yellow and red domains) in the immediate vicinity of the S4 segment of the VSD. In contrast, POPC lipids do not aggregate near the S4 segment.

stable interactions with the buried ARG (R123). While the interaction in Fig. 3b is still stable till 1000 ns, interaction in Fig. 3c, is stable for the entire duration and undergoes minimal fluctuations. Overall, these results demonstrate that while POPA-ARG interactions are stochastic in nature, POPA is able to interact with all three ARGs, including R123, over a significant period of time.

3.2 POGG and POPI lipids exhibit weak electrostatic interactions with both surface and buried ARGs

Fig. 2 and Fig. 3 show that POPA lipids preferentially aggregate near VSDs because of direct electrostatic interactions between the negatively charged headgroup and the positively charged ARG residues. However, if the charge interactions were the sole rea-

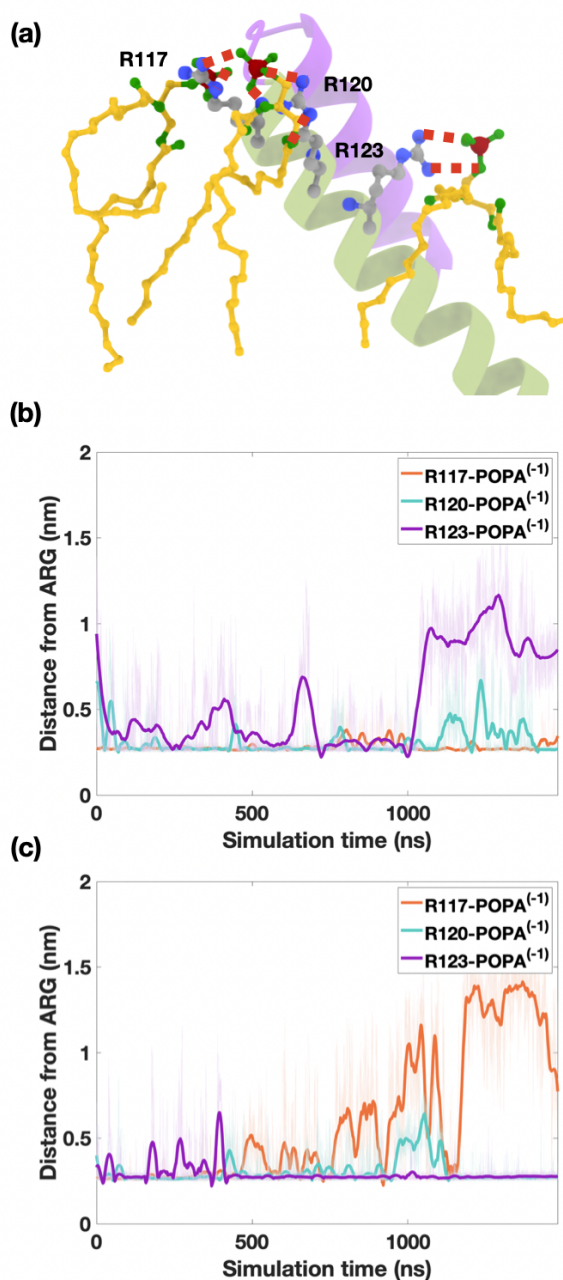


Fig. 3 MD simulations reveal POPA-ARG electrostatic interactions. (a) MD frame shows 3 POPA lipids interacting with 3 ARGs R117, R120, and R123. POPA lipids are in gold, phosphorus and oxygen atoms of POPA are in green, and nitrogen atoms of guanidinium side chains are in blue. The electrostatic interaction between ARG side chains and lipid oxygen atoms are highlighted in red dash lines. (b and c) Plot show minimum distance between any of the POPA oxygen atoms and any of the nitrogen atoms of the guanidinium side chains. We have presented results from two independent simulation in b and c to show the variations and similarities in the interactions. POPA-R117 (orange) and POPA-R120 (cyan) interactions are stable in b, while POPA-R120 (orange) and POPA-R123 (cyan) interactions are stable in c.

son for solvation, any lipid with a similar negative charge should be able to solvate the VSD. To test this conjecture, we repeated our analysis for mixed bilayers comprising of 75% POPC and 25% POPG lipids, and 75% POPC and 25% POPI lipids. The density

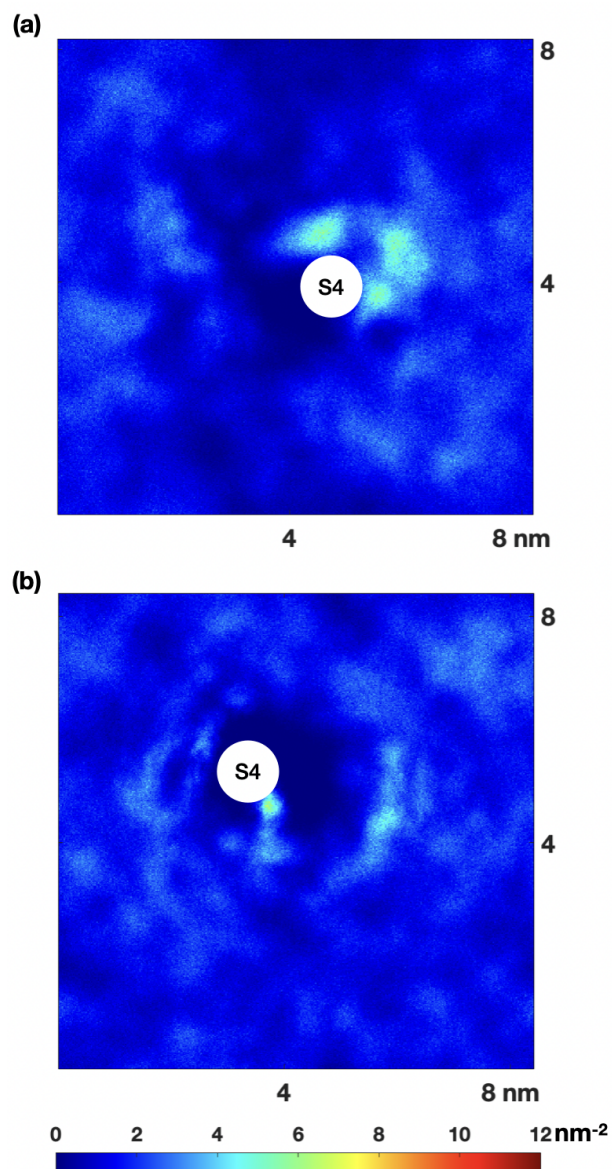


Fig. 4 2D density plot of (a) POPG and (b) POPI lipids. The two plots do not exhibit any yellow or red hotspots, as were seen in Fig. 3. This suggests that both the POPG lipids and the POPI lipids, despite having the same unit negative charge, are not able to establish strong electrostatic interaction with the S4 segment of the VSD.

plots for the POPG and POPI lipids are shown in Fig. 4a and Fig. 4b, respectively. The two plots in Fig. 4 reveal that unlike POPA, both POPG and POPI do not exhibit density hotspots in the inner solvation shell of the VSD (no yellow or red regions are seen). This suggests that despite the same charge, POPG and POPI lipids exhibit much weaker electrostatic interactions with the ARG residues, which results in a reduced solvation of the VSD. The 2D number density plots of POPG and POPI lipids from the reproduction runs are shown in Fig. S3 (ESI[†]).

To further investigate the above finding, we quantified the specific interactions between POPG and POPI lipids with the VSD. Fig. 5a and Fig. 5b show O-N distance time plots for POPG and POPI lipids, respectively. These plots reveal much larger fluctu-

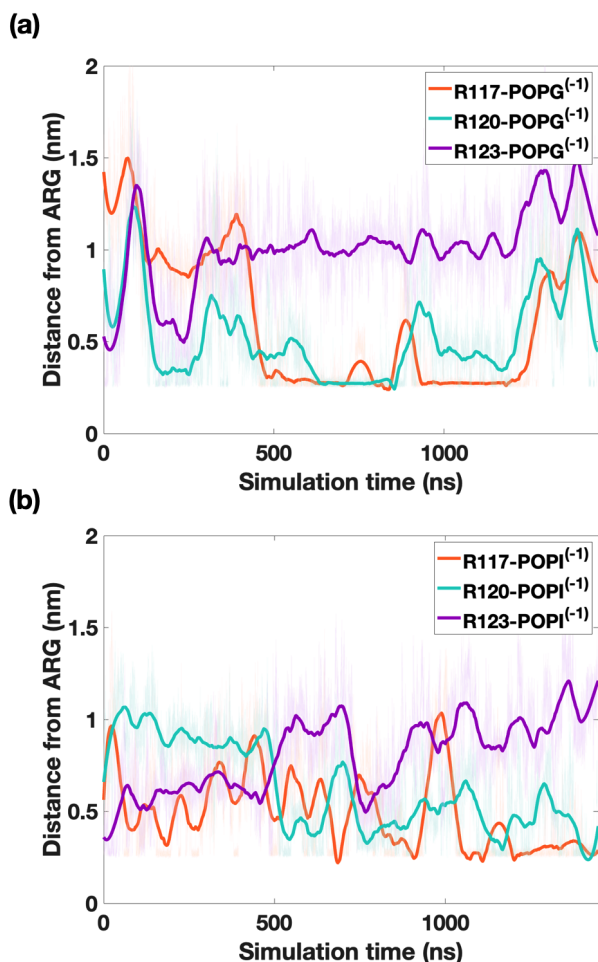


Fig. 5 Minimum distance between oxygen atoms of POPG lipids (a) and POPI lipids (b) lipids, and nitrogen atoms of guanidinium side chains of R117 (orange), R120 (cyan) and, R123 (purple). In comparison to Figs. 3(b) and 3(c), the distance-time plots much higher fluctuations. This reveals weak electrostatic interactions between the S4 segment and the POPG and POPI lipids, and explains reduced aggregation of these lipids in Fig. 4.

ations compared to those in Fig. 3b and Fig. 3c, showing that POPG lipids and POPI lipids have much weaker electrostatic interactions with the three ARGs compared to POPA lipids. This in turn shows that negative charge alone is not the determinant of stable electrostatic interactions with the ARGs but other physical parameters of the lipids can control the overall interactions. The minimum distance calculations for the reproduction runs are shown in Fig. S4 (ESI[†]).

3.3 POPA with two negative charges breaks a salt bridge connection in VSD proteins

Next, we investigated the other possibility which could further enable POPA lipids to preferentially interact with the VSD and influence channel gating. It is known that POPA lipids undergo deprotonation above a pH of 7.9^{19–21}. This environment typically exists in the vicinity of proteins with multiple basic residues under biological conditions. Thus, it is feasible that POPA lipids could undergo deprotonation in the proximity of charged pro-

teins, thereby exhibiting two negative charges. To quantify the effect of this increased charge on POPA-VSD interaction, we simulated a bilayer comprising of 90% POPC lipids and 10% POPA lipids with each POPA lipid carrying two negative charges. We did not perform similar analysis for POPG and POPI lipids as similar deprotonation has not been documented for them, to the best of our knowledge. The partial charges of the phosphate headgroup in the force field was modified to accommodate the additional negative charge. The modified partial charge distribution is given in Fig. S5a (ESI[†]).

Fig. 6a shows the density profile of POPA lipids around the VSD. We see emergence of three red colored hotspots showing POPA localization close to S4 segment. These hotspots have stronger color intensity compared to those for POPA with a unit negative charge in Fig. 3. This is so because POPA has stronger electrostatic bonds with ARGs and hence, undergo reduced spatial fluctuations. The additional hotspot that appears far away from S4 is due to the clustering of POPA lipids due to two negative charges. In addition to electrostatic interactions with arginines, propensity to form domain might be contributing to the strengthening of the three hotspots near the S4 segment. Fig. 6b shows an image of POPA lipids interacting with the ARGs (blue). The figure reveals that the POPA lipids have formed electrostatic bonds with ARGs R117, R120 and R123. Fig. 6c shows distance between the POPA headgroup oxygen atoms and nitrogen atoms in the ARG guanidinium side chains. We observe that the time plots are much flatter for POPA lipids with -2 charge, once they enter the solvation shell of VSD. In addition, POPA lipids are able to maintain electrostatic interactions all the arginines, including R123, concurrently. The 2D number density of the POPA⁽⁻²⁾ lipid reproduction run is shown in Fig. S5b (ESI[†]).

Going beyond O-N distance plots, we also analyzed the distance between R123 and glutamic acid E107 (a counter charge on the neighboring S3b segment of the VSD) in Fig. 7a. The plot reveals a remarkable switch undergone by R123 around 1000 ns. The salt bridge connection between R123-E107 gets broken and a new electrostatic connection is established between R123-POPA⁽⁻²⁾. This is reflected in the fact that the green curve rises and the magenta curve comes down around the same time. This is novel since R123 forms a salt bridge with E107 in all the previous simulations, including those for POPA with unit negative charge. We confirmed this finding by measuring R123-POPA and R123-E107 distances. In all the previous simulations R123 maintains a minimum distance of around 0.3 nm with E107. In the case of POPA with -2 charges, R123-E107 minimum distance increases to 0.6 nm and the R123-POPA minimum distance reduces to 0.3 nm. This suggests that the POPA lipid with -2 charges is able to break the salt bridge connection and establish its own electrostatic bond with R123. Thus, deprotonation of POPA lipids is able to allow POPA lipids to establish stronger electrostatic interactions with Kv channels. Fig. 7b shows the overlapped snapshots of the S4-S3-POPA system prior to and after the switch. The side chain containing R123 rotates to let go of its salt-bridge connection with E107 and establish a new electrostatic bond with POPA⁽⁻²⁾. The ARG-lipid time plots and salt bridge plots for the second production run are shown in Fig. S6 (ESI[†]).

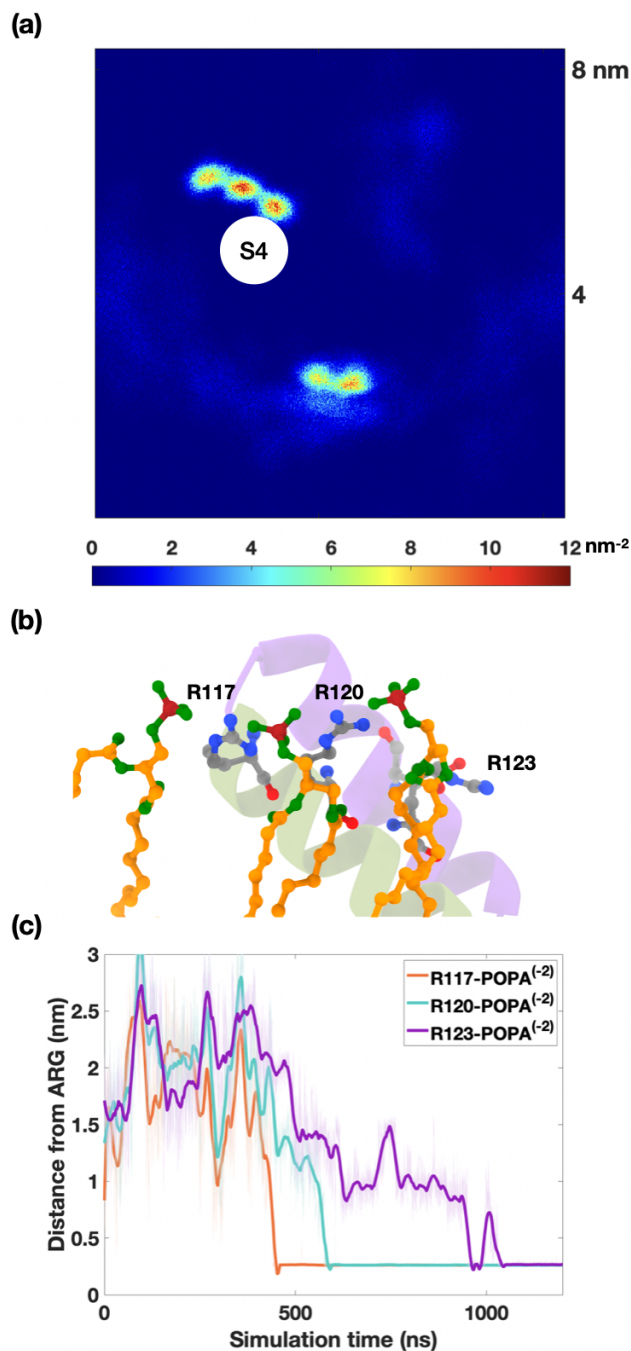


Fig. 6 POPA with -2 charges show strong electrostatic interactions with the VSD. (a) 2D density plot showing three POPA hotspots near the S4 segment. The other two hotspots away from the S4 segment occur because of POPA clustering triggered by double negative charges. Similar effect could be contributing to the formation and stability of the three hotspots near the S4 segment. (b) A typical frame from the MD simulation shows three POPA lipids (orange) in the close proximity of the S4 segment. (c) After initial fluctuations, POPA lipids with -2 charges show very stable electrostatic interactions with all three arginines simultaneously: R117 (orange), R120 (cyan), and R123 (purple).

4 Discussion

In this study, we performed molecular dynamics simulations to investigate the interactions of anionic lipids with the VSD of KvAP

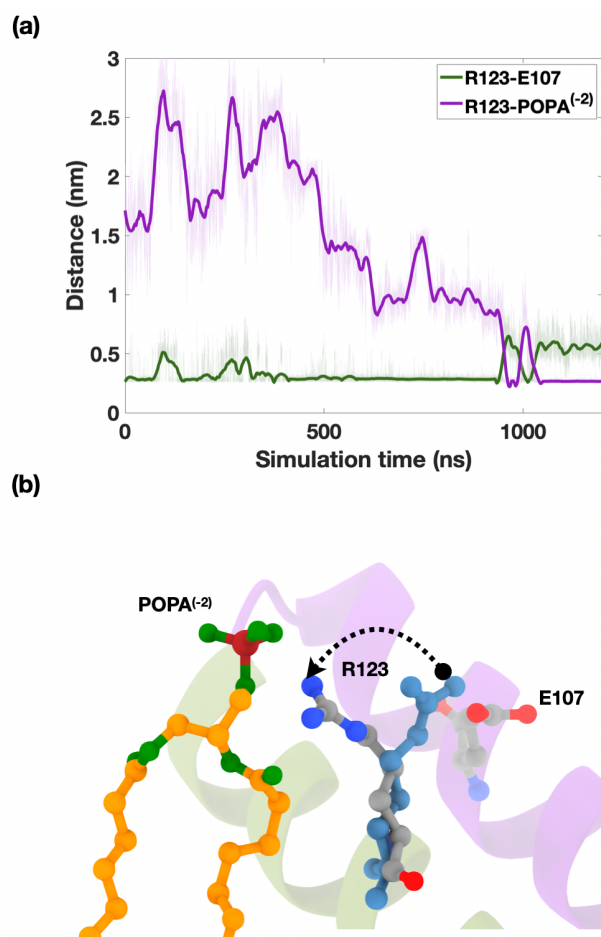


Fig. 7 POPA with -2 charge breaks salt-bridge connection. (a) Minimum distance plots between arginine R123 and glutamic acid E107 (green), and R123 and POPA with -2 charge (purple). Around 1000 ns, the green curve rises to a higher distance and simultaneously, the purple curve stabilizes at a smaller distance. This demonstrates that the electrostatic interaction between R123-E107 is replaced with that between R123-POPA. (b) Overlapped images of S4-S3-POPA system before and after the switch shows that the arginine side chain undergoes rotation, which results in breakage of the salt-bridge connection and formation of the POPA-R123 bond.

channel as a model system. Our study reveals that POPA is able to snorkel into the headgroup region and interact with the buried arginine R123. On the other hand, POPG and POPI lipids are unable to snorkel and interact with R123 in the simulated time frame. In addition, their interactions with the surface ARGs are also much weaker compared to that of POPA. This suggests that despite a similar charge, POPA has a higher propensity to establish electrostatic interactions with the arginines than POPG and POPI lipids. Our study also shows that deprotonated POPA with -2 charge is able to break a salt bridge connection (R123-E107) and establish its own electrostatic connection with the positive residue. Fig. 8 shows a schematic that summarizes these findings. These interactions might be at play in cellular processes where POPA acts as a signaling lipid and interacts with charged transmembrane proteins. KvAP VSD serves as a model system and the electrostatic interactions identified in this study should be ap-

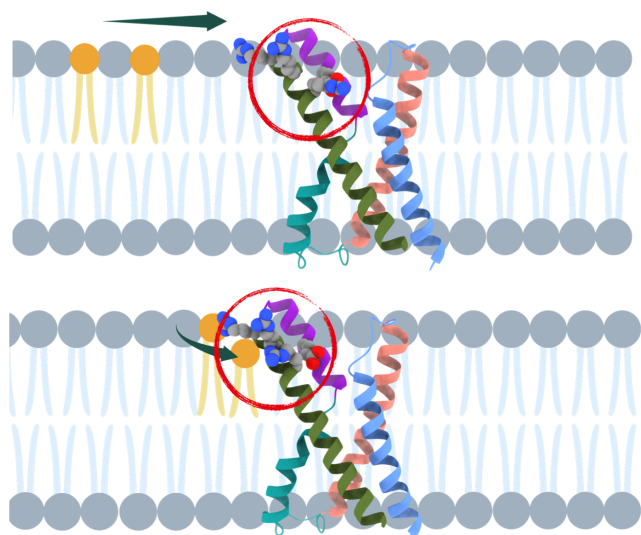


Fig. 8 Schematic showing ARG-POPA interactions. POPA aggregates around ARG residues in the VSD. POPA is able to snorkel and interact with the buried arginine R123, and POPA⁽⁻²⁾ is able to break the salt bridge between R123 and E107 (in red).

plicable to any charged protein buried in a bilayer comprised of anionic lipids.

4.1 Headgroup size hypothesis for lipid-protein interactions

We can analyze the structural properties of POPA, POPG and POPI lipids to gain further insights into the relative electrostatic interactions they exhibit with VSD ARGs. A comparison of the headgroup sizes of POPA, POPG and POPI lipids show that POPA lipids have 35% and ~60% smaller volume than POPG and POPI lipids, respectively (see Fig. S8, ESI†)³⁵⁻³⁹. While POPA has a hydrogen ion linked to the phosphate group, POPG has a glycerol group connected to the phosphate group, and POPI has an inositol group connected to the phosphate group, resulting in bigger headgroup sizes and a lower charge density. As POPA, POPG and POPI lipids have identical acyl chains, the fact that POPG and POPI lipids are not able to establish strong interaction with R123 can potentially be attributed to a bigger headgroup size. This conjecture is also supported by the fact the POPG and POPI lipids exhibit much larger fluctuations, even with respect to the surface ARGs R117 and R120 (please see Fig. 5). This encourages us to propose a lipid headgroup size hypothesis, which suggests that the size of headgroup may be a critical parameter that determines the strength of lipid-protein interactions and the extent to which lipids are able to solvate proteins.

4.2 Umbrella sampling simulations suggest strong interactions of POPA with buried ARG

In order to gain deeper insight into the interactions of anionic lipids with arginines, we performed umbrella sampling simulations. Following the approach of Sansom and co-workers⁴⁰⁻⁴³, we pulled the bound lipids away from the ARGs in a radially out-

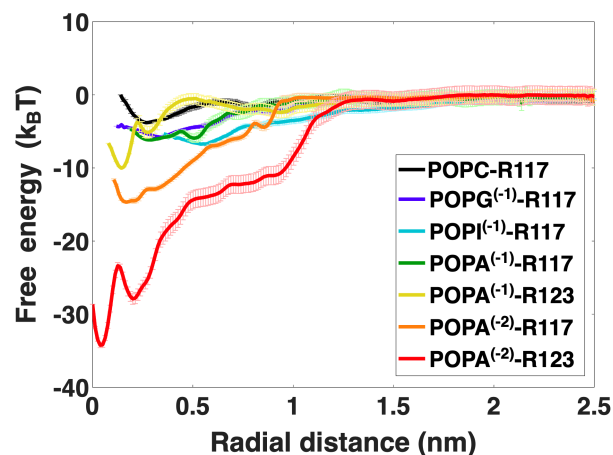


Fig. 9 Free energy curves for lipid-arginine interactions. POPC lipid has the shallowest energy well, followed by energy wells for anionic lipids with unit negative charge interacting with the surface arginine R117 (POPA green curve, POPG purple curve, and POPI cyan curve). Interactions with all three lipids have similar well depths. In contrast, interaction of POPA with buried arginine R123 has a deeper well (yellow curve). Presence of -2 charge on POPA significantly lowers the energy wells for interactions with both the surface arginine R117 (orange curve) and buried arginine R123 (red curve).

ward direction in a sequence of steps and computed the free energy curves. The details of the method are described in the SI. Since we pull the lipids in the radial direction alone, orthogonal degrees of freedom are suppressed. As a result, the free energy curves obtained are 1-D projection of a rugged energetic landscape. Nonetheless, these energy calculations provide a qualitative insight into the strength and specificity of anionic lipids with arginines under identical numerical setup.

Fig. 9 shows the free energy curves for POPA with -2 charge bound to R117 and R123, POPA with -1 charge bound to R117 and R123, POPG bound to R117, POPI bound to R117, and POPC bound to R117. We can observe that depths of the energy wells for anionic lipids with a -1 charge interacting with R117 are nearly the same and are slightly deeper than that for POPC lipids because of stronger electrostatic interactions. The depth of the energy well for POPA with -1 charge interacting with R123 (orange curve) is deeper than the wells associated with surface arginine (yellow curve). This demonstrates that snorkeling enables POPA lipid to achieve an increased energetic gain. The same trend is seen in the cases of POPA lipids with -2 charges interacting with R117 and R123. The energetic gain is much higher for interactions with buried arginine (red curve) than surface arginine (orange curve). In addition, as per expectations, -2 charge lowers the energy wells significantly compared to the wells obtained with -1 charge (compare orange and green curves, and red and yellow curves). Overall, this analysis reveals that the interactions with the buried arginine offers a larger energetic gain compared to that obtained from surface arginine. Since POPA is able to forge these electrostatic interactions, it gives them greater capability to influence protein kinematics.

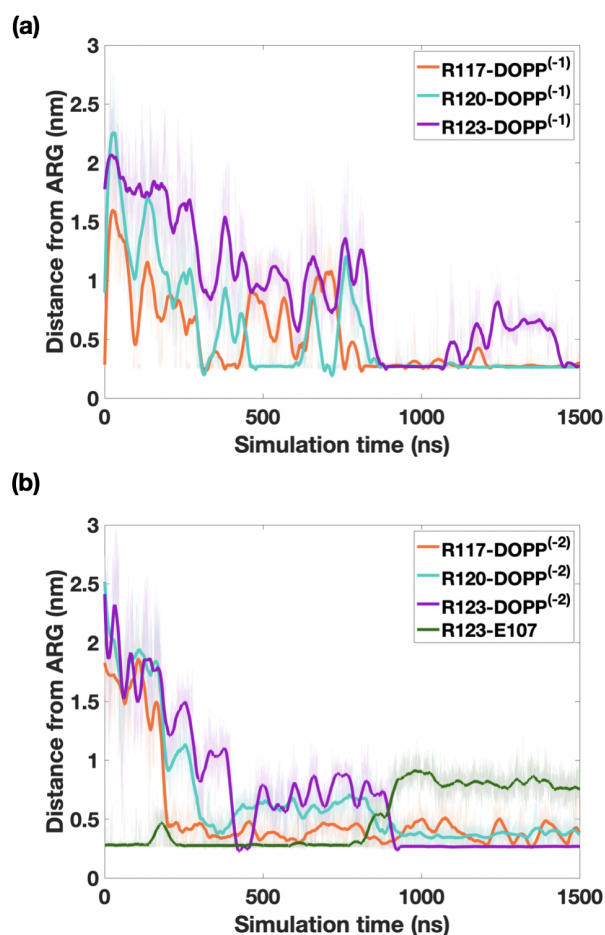


Fig. 10 MD simulations reveal S4-DOPP interactions, similar to exhibited by POPA lipids. (a) Minimum distance plots demonstrate that DOPP lipids with -1 charge are able to maintain stable interactions with R117 and R120. (b) Minimum distance plot reveals that DOPP with -2 charge is able to break R123-E107 salt-bridge connection and establish its own electrostatic bond with R123. The transition between the green and purple curves happen simultaneously as was observed for POPA lipids with -2 charge.

4.3 Reproducibility and robustness of the findings

In addition to running multiple independent simulations, we validated our findings by modeling another VSD-bilayer system that comprised of 75% POPC lipids and 25% DOPP lipids. DOPP lipids are similar to POPA lipids with a small headgroup size and exist with both -1 and -2 charges. Experimental studies also show that DOPP lipids have significant effect on KvAP gating⁴. Fig. 10 shows the ARG-DOPP distance time plots for systems with DOPP with -1 charge and DOPP with -2 charge. Fig. 10a shows that similar to POPA, DOPP with -1 charge is able to establish electrostatic interactions with the two surface arginines. Fig. 10b shows that DOPP with -2 charge shows similar interactions with ARGs as POPA with -2 charge. DOPP is able to break the R123-E107 salt bridge connection and establish its electrostatic bond with R123. As for POPA, the switch in the electrostatic interactions between R123-E107 to R123-DOPP happen simultaneously. These additional analyses confirm that our findings are robust and tied to the physical properties (charges and geometry) of the lipids.

Abbreviations

KvAP: Kv channel from the thermophilic archaea *Aeropyrum pernix*

VSD: Voltage Sensor Domain

POPA: 1-hexadecanoyl-2-(cis-9-octadecenoyl)-sn-glycero-3-phosphate (1-Palmitoyl-2-oleoyl-sn-glycero-3-phosphate)

POPC: 1-hexadecanoyl-2-(9Z-octadecenoyl)-sn-glycero-3-phosphocholine (1-Palmitoyl-2-oleoyl-sn-glycero-3-phosphocholine)

POPG: 1-hexadecanoyl-2-(cis-9-octadecenoyl)-sn-glycero-3-phospho-(1'-sn-glycerol) (1-Palmitoyl-2-oleoyl-sn-glycero-3-phosphoglycerol)

POPI: 1-hexadecanoyl-2-(cis-9-octadecenoyl)-sn-glycero-3-phospho-1D-myo-inositol (1-Palmitoyl-2-oleoyl-sn-glycero-3-phosphoinositol)

DOPP: 1,2-dioctadec-9-enoyl-sn-glycero-3-phosphate (1,2-dioleoyl-sn-glycero-3-phosphate)

Author contributions

A.A. conceived the study, N.T, K.K.M. and A.A. designed the MD simulations, N.T. and W.C. carried out the atomistic simulations, N.T, K.K.M. and A.A. analyzed the data and wrote the manuscript.

Conflicts of interest

There are no conflicts to declare.

Acknowledgments

We would like to acknowledge Dr. Mehdi Torbati for scientific discussions. This work was supported by National Science Foundation Grants CMMI 1562043, CMMI 1727271 and CMMI 1931084 to A.A.. K.K.M was supported by Director, Office of Science, Office of Basic Energy Sciences, of the U.S. Department of Energy under contract No. DEAC02-05CH11231. The authors also acknowledge the use of the Maxwell/Opuntia/Sabine Clusters and the advanced support from the Research Computing Data Core at UH to carry out the research presented here.

References

- 1 K. Athenstaedt and G. Daum, *European Journal of Biochemistry*, 1999, **266**, 1–16.
- 2 J. J. Shin and C. J. Loewen, *BMC biology*, 2011, **9**, 85.
- 3 D. M. Raben and C. N. Barber, *Advances in biological regulation*, 2017, **63**, 15–21.
- 4 R. K. Hite, J. A. Butterwick and R. MacKinnon, *Elife*, 2014, **3**, e04366.
- 5 M. Raja, R. E. Spelbrink, B. de Kruijff and J. A. Killian, *FEBS letters*, 2007, **581**, 5715–5722.
- 6 Y. Comoglio, J. Levitz, M. A. Kienzler, F. Lesage, E. Y. Isacoff and G. Sandoz, *Proceedings of the National Academy of Sciences*, 2014, **111**, 13547–13552.
- 7 E. B. Riel, B. C. Jürs, S. Cordeiro, M. Musinszki, M. Schewe and T. Baukrowitz, *Journal of General Physiology*, 2021, **154**, e202112989.
- 8 P. A. Schmidpeter, D. Wu, J. Rheinberger, P. M. Riegelhaupt,

- H. Tang, C. V. Robinson and C. M. Nimigean, *Nature structural & molecular biology*, 2022, **29**, 1092–1100.
- 9 S. Schrecke, Y. Zhu, J. W. McCabe, M. Bartz, C. Packianathan, M. Zhao, M. Zhou, D. Russell and A. Laganowsky, *Nature chemical biology*, 2021, **17**, 89–95.
- 10 P. A. Schmidpeter, J. T. Petroff, L. Khajouejinejad, A. Wague, C. Frankfater, W. W. Cheng, C. M. Nimigean and P. M. Rieghaupt, *Nature communications*, 2023, **14**, 1077.
- 11 M. Raja, *Journal of Membrane Biology*, 2010, **234**, 235–240.
- 12 M. Raja, *The Journal of membrane biology*, 2014, **247**, 747–752.
- 13 Z.-R. Zhang, C.-F. Chou, J. Wang, Y.-Y. Liang and H.-P. Ma, *Pflügers Archiv-European Journal of Physiology*, 2010, **459**, 377–387.
- 14 P. Marius, S. J. Alvis, J. M. East and A. G. Lee, *Biophysical journal*, 2005, **89**, 4081–4089.
- 15 S. S. Deol, C. Domene, P. J. Bond and M. S. Sansom, *Biophysical journal*, 2006, **90**, 822–830.
- 16 J. A. Poveda, A. M. Giudici, M. L. Renart, O. Millet, A. Morales, J. M. González-Ros, V. Oakes, S. Furini and C. Domene, *Biochimica et Biophysica Acta (BBA)-Biomembranes*, 2019, **1861**, 183029.
- 17 J. F. Neal, W. Zhao, A. J. Grooms, A. H. Flood and H. C. Allen, *The Journal of Physical Chemistry C*, 2018, **122**, 26362–26371.
- 18 H. Zhou, Y. Huo, N. Yang and T. Wei, *The FEBS Journal*, 2023.
- 19 J. Zegarliniska, M. Piascik, A. F. Sikorski and A. Czogalla, *Acta Biochimica Polonica*, 2018, **65**, 163–171.
- 20 E. E. Kooijman, K. M. Carter, E. G. Van Laar, V. Chupin, K. N. Burger and B. De Kruijff, *Biochemistry*, 2005, **44**, 17007–17015.
- 21 E. E. Kooijman, D. P. Tieleman, C. Testerink, T. Munnik, D. T. Rijkers, K. N. Burger and B. De Kruijff, *Journal of Biological Chemistry*, 2007, **282**, 11356–11364.
- 22 D. O. Kwarteng, M. Gangoda and E. E. Kooijman, *Biophysical Chemistry*, 2023, **296**, 107005.
- 23 B. P. Young, J. J. Shin, R. Orij, J. T. Chao, S. C. Li, X. L. Guan, A. Khong, E. Jan, M. R. Wenk, W. A. Prinz *et al.*, *Science*, 2010, **329**, 1085–1088.
- 24 A. Bhushan and M. G. McNamee, *Biophysical journal*, 1993, **64**, 716–723.
- 25 J. Faraudo and A. Travasset, *Biophysical journal*, 2007, **92**, 2806–2818.
- 26 E. E. Kooijman and K. N. Burger, *Biochimica et Biophysica Acta (BBA)-Molecular and Cell Biology of Lipids*, 2009, **1791**, 881–888.
- 27 E. Tanguy, N. Kassas and N. Vitale, *Biomolecules*, 2018, **8**, 20.
- 28 S. Jo, T. Kim, V. G. Iyer and W. Im, *Journal of computational chemistry*, 2008, **29**, 1859–1865.
- 29 S. Jo, J. B. Lim, J. B. Klauda and W. Im, *Biophysical journal*, 2009, **97**, 50–58.
- 30 X. Tao and R. MacKinnon, *Elife*, 2019, **8**, year.
- 31 J. Lee, X. Cheng, J. M. Swails, M. S. Yeom, P. K. Eastman, J. A. Lemkul, S. Wei, J. Buckner, J. C. Jeong, Y. Qi *et al.*, *Journal of chemical theory and computation*, 2016, **12**, 405–413.
- 32 J. Huang, S. Rauscher, G. Nawrocki, T. Ran, M. Feig, B. L. de Groot, H. Grubmüller and A. D. MacKerell, *Nature methods*, 2017, **14**, 71–73.
- 33 S. Boonstra, P. R. Onck and E. van der Giessen, *The journal of physical chemistry B*, 2016, **120**, 3692–3698.
- 34 D. Van Der Spoel, E. Lindahl, B. Hess, G. Groenhof, A. E. Mark and H. J. Berendsen, *Journal of computational chemistry*, 2005, **26**, 1701–1718.
- 35 K. Harlos, H. Eibl, I. Pascher and S. Sundell, *Chemistry and physics of lipids*, 1984, **34**, 115–126.
- 36 I. Pascher, S. Sundell, K. Harlos and H. Eibl, *Biochimica et Biophysica Acta (BBA)-Biomembranes*, 1987, **896**, 77–88.
- 37 I. Pascher and S. Sundell, *Chemistry and physics of lipids*, 1992, **62**, 79–86.
- 38 D. Marsh, *Chemistry and physics of lipids*, 2010, **163**, 667–677.
- 39 J. P. DiNitto, T. C. Cronin and D. G. Lambright, *Science's STKE*, 2003, **2003**, re16–re16.
- 40 G. Hedger, D. Shorthouse, H. Koldsø and M. S. Sansom, *The Journal of Physical Chemistry B*, 2016, **120**, 8154–8163.
- 41 J. Domański, G. Hedger, R. B. Best, P. J. Stansfeld and M. S. Sansom, *The journal of physical chemistry B*, 2017, **121**, 3364–3375.
- 42 W. Song, H.-Y. Yen, C. V. Robinson and M. S. Sansom, *Structure*, 2019, **27**, 392–403.
- 43 T. B. Ansell, R. A. Corey, L. V. Viti, M. Kinnebrew, R. Rohatgi, C. Siebold and M. S. Sansom, *Science Advances*, 2023, **9**, eadh1609.